Addition of Lithium Silylamides to 1,2-dicyanobenzene; Isoindoline-1,3-diimine Derivatives Investigated by NMR/XRD/DFT Approach

Stanislava Majerová,[†] Tomáš Chlupatý,[†] Maksim A. Samsonov,[†] Josef Cvačka,[ǁ] Eliška Procházková,[ǁ*] Aleš Růžička[†*]

[†]Department of General and Inorganic Chemistry, Faculty of Chemical Technology, University of Pardubice, Studentská 573, Pardubice 532 10, Czech Republic
[ǁ]Institute of Organic Chemistry and Biochemistry, Czech Academy of Sciences, Flemingovo nám. 2, Prague 160 00, Czech Republic
*Eliška Procházková –prochazkova@uochb.cas.cz, Aleš Růžička – ales.ruzicka@upce.cz

KEYWORDS. Lithium amides; phthalocyanines; diiminoisoindoles; guanidinates;

ABSTRACT: Phthalocyanines and its building blocks – isoindoline-1,3-diimines (diiminoisoindoles, DIIs), represent a structurally-diverse class of compounds with ability to make metal complexes and perform in various fields from medicine to photovoltaics and homogenous catalysis. According to the present study monosubstituted diiminoisoindoles, their higher homologues, and complexes can be effectively prepared by an addition of silylated lithium amides to 1,2-dicyanobenzene followed by mild protonolysis or a condensation. An addition of DII to carbodiimides or reactions of lithiated DIIs with acylchlorides give DII-guanidines and amido derivatives. The imino group of the amido derivatives is preferentially and quantitatively reduced by sodium borohydride. Dynamic behavior and structure of all studied classes of compounds were investigated from the stereochemical point of view – possible *E*/*Z*-isomerization and dimerization (DIIs and amido derivatives), tautomerism (guanidines) and stability both in solution as well as in solid state. The resonance-assisted hydrogen bonds are present in all species, except reduced amides, predetermining them to be exceptional ligands in coordination chemistry.

Introduction

Phthalocyanines (PC) are nitrogen rich, planar, aromatic compounds, with a lot of possible substitutional patterns. Their versatility, thermal robustness, supramolecular assembly and electronic structure are reflected in a wide range of applications such as dyes and pigments or in photoelectricity. Doubly deprotonated PCs are perfect macrocyclic ligands capable of accommodating almost all metals from the periodic table in a plethora of bonding motifs. Taking into the account tunable electronic and optical properties, coupled with stability, some of these complexes were identified as invaluable species for organic electronics, catalysis and medicinal chemistry[1]. Virtual building blocks of PCs are undoubtedly the isoindoline-1,3-diimine (DII) derivatives, from which additionally starts a synthesis of many PCs (Fig. 1).

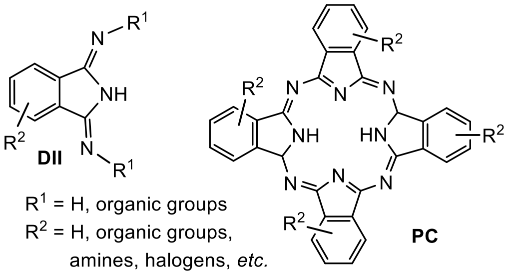

Figure 1. Structures of DIIs and PCs.

Although the chemistry and applications of PCs could be seen as the major purpose of DIIs studies, they are also involved as construction parts in a plethora of materials. Biologically active species and their isoindole fragments can be found in number of natural products[2] and dyes[3]. Concretely, they are used for synthesis of phthalocyanine analogues such as hemiporphyrazines, hydroxybenzipthalocyanines or biliazine[4–7], synthesis of fluorophores BOSHPY (BODIPY analogues)[8,9], design of anion receptors[10] and electrocatalysts for oxygen evolution[11]. Mentionable from biologically active compounds are C3a antagonists[12] and antimalarial candidates[13].

Various DIIs and vast majority of derivatives have been prepared from 1,3-diiminoisoindoline and primary amines, following the seminal work of Linstead, who was the first to describe this condensation reaction almost 70 years ago[14,15]. In order to increase the yields of both symmetrical (bis-derivative) and dissymmetrical species, several modifications of that method appeared. Much later, Siegl and others addressed the same issue, finding that phthalonitrile adds anilines, specifically to bis-1,3-(arylimino)isoindoline, when reactions are catalyzed by anhydrous calcium chloride[16–18]. They were followed by Ziegler, who reinvestigated the preparation of bis-1,3-(arylimino)isoindoles and bis-1,3-(alkylimino)isoindoles both in the solid state and in solution[19]. All methods are characterized by long reaction times, significantly increased temperature, low to moderate yields, necessity of a catalyst and challenging purification with necessary workup by recrystallization or flash chromatography.

Surprisingly, not that many metal complexes containing DIIs and its derivatives (excluding PCs) have been prepared thus far. Majority of coordination compounds containing DII moiety are on the basis of using 2-pyridyl (or similar) substituents. These allow the use of DII part as a terdentate ligand using one isoindole nitrogen atom and two auxiliary pyridyl nitrogens in a planar fashion. Such complexes of transition metals, prepared mainly by Gade[20–23], Ziegler[24,25] and others, are further used as epoxidation or hydrogenation catalysts. Besides that, Ziegler used rhenium ion as a template for preparation of condensed DII compounds[26], Sanford investigated Ni complexes as potential anolyte materials used in nonaqueous redox flow batteries[27] and Bochkarev synthesized structurally interesting series of rare earth metals complexes[28].

This paper describes a novel approach to synthesis of variously substituted dissymmetrical DIIs, by similar reaction as described earlier for amidinates[29–33]. In the first part, there is a description of reaction pathways with crystallographically determined structures of key complexes and byproducts. In the second part the reactivity of monosubstituted DIIs is reported to synthesize compounds usable as ligands for various metals, including investigation of their molecular dynamics and isomerism in solid state and solution.

Results and Discussion

Synthesis and Characterization of Lithium complexes

As a part of our research program, one of the possible synthetic strategies for main group metal amidinates,addition of silylated lithium amide to nitrile group[29–31], has been explored for (oligo)nitriles with aliphatic chain as well as several di- up to tetracyanobenzenes[32,33].

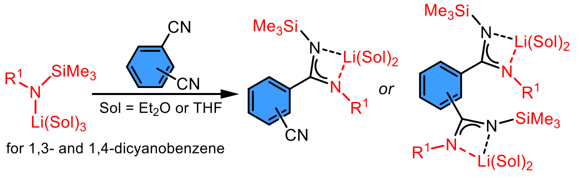

Scheme 1. Method for synthesis of lithium amidinates from lithium amides and dicyanobenzenes[33], Sol = THF or diethyl ether.

In the series of dicyanobenzenes, the 1,3- and 1,4-derivatives gave, according to the stoichiometry, desired lithium nitriloamidinates and dilithium bisamidinates (Scheme 1)[33]. Inspired by these transformations, we carried out the reaction of one equivalent of 1,2-dicyanobenzene[33] with several trimethylsilylated lithium amides. In strong contrast to reactions of 1,3- and 1,4-dicyanobenzene it gives cyclization products - lithium 1-(trimethylsilylimino)-3-(arylimino)isoindolines in high yields (Scheme 2). An addition of lithium amide to unsaturated nitrile bond followed by a migration of the trimethylsilyl group and ring closure is a logical explanation of the process. According to ^{1}H and ^{13}C NMR spectra, it seems the complete conversion is accomplished within a couple of hours at room temperature. The ^{1}H and ^{13}C NMR spectra of all lithium complexes are in line with spectral assignments made by Spiessens or Ziegler[16–19] for alkyl- or aryliminoisoindolines. Only the ^{13}C signals of endocyclic carbon atoms C1 and C7a (see the Supplementary Information) are shifted to lower field by ~ 7 ppm and ~ 5 ppm, respectively, which can be attributed to influence of lithium coordination. Thanks to symmetrical structure of Li**1e**, we can observe only three broader signals in the ^{1}H NMR spectra in THF-d_8, namely the aromatic hydrogens of isoindole and the trimethylsilyl group with the corresponding integral intensity. There are five ^{13}C signals that can be unambiguously assigned to the isoindole unit and the $SiMe_3$ groups. In the ^{29}Si NMR spectrum, one resonance of the $SiMe_3$ group at -8 ppm is observed similarly as in the ^{7}Li NMR spectrum, where relatively narrow signal occurs at 1.1 ppm.

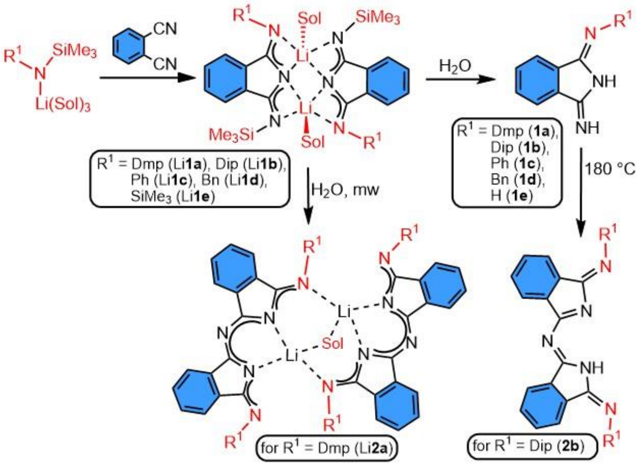

Scheme 2. Observed reactivity of silylated lithium amides to DIIs; Dmp = 2,6-dimethylphenyl-; Dip = 2,6-diisopropylphenyl-; Sol = THF, diethyl ether, mw = microwave reactor.

Lithium complexes Li**1a** and Li**1b** (Scheme 2) were crystallized as the single crystalline materials in the first crop from the reaction mixture with yields about 65%. Both complexes are dimeric with nearly planar arrangement of isoindoline rings (Fig. 2, S47). Each of two lithium atoms, which are ~ 0.5Å below and above the central plane, connecting two endocyclic and two exocyclic nitrogen atoms of both isoindoline moieties. Thus, the lithium atoms are found in unusual geometry of nearly perfect square pyramid as found only for some lithium porphyrinoids[34]. Dmp and Dip groups in Li**1a** and Li**1b** are perpendicularly oriented to the central plane. The interatomic distances and angles between lithium and nitrogen or oxygen atoms are in line with similar type of distances previously found in structures of dissymmetric trimethylsilyl substituted lithium amidinates[23,24]. On the other hand, interatomic distances found in the ligand (see Fig. 2) clearly demonstrate that double bonds are located at the peripheral imino groups and thus a delocalized character of NCN chelating unit in amidinates is not taking place in lithium diiminoisoindolines Li**1a** and Li**1b**.

Low quality of Li**1c**, Li**1d** and Li**1e** crystals were not suitable for structure determination by sc-XRD, but an interesting adduct of dinuclear Li**1e** with partially hydrolyzed species was crystallized as fortuitous minor material (see SI, Fig. S72). This adduct consists of four diiminoisoindoline units, two of them are partially hydrolyzed which is manifested by the replacement of one $SiMe_3$ substituent with a hydrogen atom. Four lithium atoms are coordinated in the structure, each by means of four diiminoisoindoline nitrogens. The N-Li interatomic distances are in the range of 2.07-2.17 Å, which are comparable with the sum of the covalent radii of nitrogen and lithium atoms of 1.99 Å [35] and similar types of separations in Li**1a** and Li**1b**.

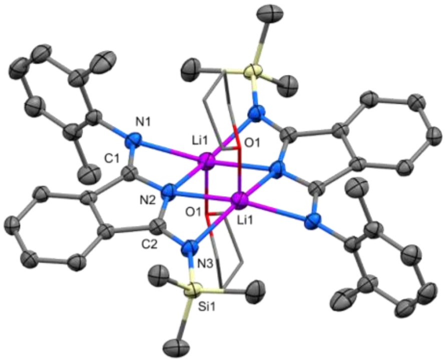

Figure 2. The molecular structure of Li**1a**, ORTEP view 50% probability level of. Hydrogen atoms are omitted for clarity, THF ligands are shown in wireframe mode. Selected bond lengths (Å) and angles (°): N1–C9 1.418(3), N1–C1 1.289(3), C1–N2 1.372(3), N2–C2 1.363(3), C2–N3 1.296(3), N3–Si1 1.713(2), N1–Li1 2.209(4), N2–Li1 2.127(4), N3–Li1 2.100(4), C1–N1–C9 120.79(18), N1–C1–C4 132.14(19), N1–Li1–N2 63.7(1), N2–Li1–N3 64.1(1). Symmetry code: -x, -y, -z.

Protonolysis of all mentioned lithium complexes occurs just by letting solutions or crystals on the air for a period of couple minutes to hours or adding non-dried solvent to the crude reaction mixture. Alkyl- or aryliminoisoindolines **1a**-**1e** can be crystallized from solutions after treatment with water in very good yields. According to the ^{1}H and ^{13}C NMR spectra in DMSO-d_6, the prepared compounds exhibit similar behavior in DMSO-d_6 solution as described by Spiessens or Shishkin for non- to symmetrically disubstituted DIIs[16–17,36–38]. The imino form A, *Z*-isomer at nitrogen atom highlighted in blue color in Scheme 3, predominates in all the compounds. In contrast to reported works, we are strongly convinced by the set of 2D NMR (COSY, HMBC and NOESY) experiments, that the tautomeric equilibrium between A and B forms does not exist in solutions of THF-d_8 and $CDCl_3$, and only the same *E*/*Z*-isomerization of diimino forms A is taking place. In addition, there is no evidence of a dimer formation (Scheme 3 C or D), suggested by other authors as a part of the tautomerization process, in solvents used. The solid proof for that statement is also the DOSY NMR measurement (Figs. S41–S42) of **1a**, which gave traces with very close diffusion coefficients for both sets of signals (for *E*- and *Z*-isomers of diamino form A) observed in the spectra. Also, the mixture of **1a** and **5ab**, which is not capable to make a dimer, was investigated by this technique in order to evaluate **1a** not being aggregated in solution.

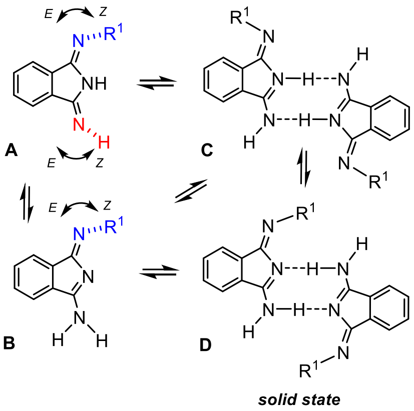

Scheme 3. Plausible isomerization pathways of dissymmetrically substituted DIIs. Monomeric (A, B) a dimeric species (C, D). Circular arrows illustrate *E*/*Z* isomerism at imino groups – *E*-isomers are shown only for dimeric species of the type C.

The molecular structures of **1a**, **1b** and **1c** determined in the solid state are the best to be described as centrosymmetric dimers. These dimers are connected by two strong H-bridges mediated by isoindole nitrogen atoms as donors of electron density and NH_2 groups as acceptors (Scheme 3, D). Structure of **1c**, previously described in literature[39], was redetermined in order to have the direct comparison with structures of **1a** and **1b** (Fig. 3). In both structures (analogously to **1c**) the acidic hydrogen atoms are unambiguously located at the terminal exocyclic nitrogen atom (Scheme 3, D), which is in contrast with the observations made in solution. The shortest distance was identified between C1 and the exocyclic nitrogen atom N1, while C2-N2 and C2-N3 are mutually comparable and significantly longer. One would expect, the hydrogen atoms will be localized as in solution at N2 (judged from the longest C1-N2 separation) and N3 atoms. But the presence of both hydrogen atoms at N3 atom prevailed probably thanks to the formation of the dimer via strong H-bonds (Fig. 3). While the structures of **1a** and **1b** exhibit planar organization of the DII fragments and perpendicular orientation of the Dmp and Dipp substituents (Fig. 3), respectively, the interplanar angle of DII groups in **1c** is 87.14(12)° most probably due to steric reasons (see SI, Fig. S55)[39]. In fact, this rather polarized arrangement found in the solid state is not in line with theoretical calculations reported elsewhere[36]. We took the opportunity to reinvestigate the dimerization of **1a** carefully.

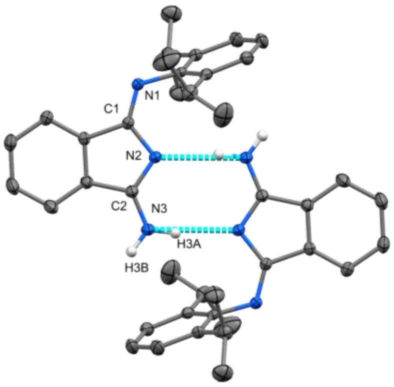

Figure 3. The molecular structure of **1b**, ORTEP view 50% probability level. Hydrogen atoms are omitted for clarity. Selected bond lengths (Å) and angles (°): N1–C9 1.4241(13), N1–C1 1.2790(13), C1–N2 1.4052(13), N2–C2 1.3309(13), C2–N3 1.3253(14), C1–N1–C9 119.70(9), N1–C1–C4 123.60(9).

It seems, the tautomer with NH_2 moiety dimerizes upon formation of both planar and perpendicular dimers (*vide supra* for structures of **1a**, **1b** and **1c**) as the lowest energy species when compared to another possible dimers and monomers by ~5 kcal/mol (for more details see SI, Figs. S1 – S2). Reason for this tautomeric rearrangement going from solution to the solid state is the stabilization of the lowest energy and optimal structure by resonance-assisted hydrogen bonding (RAHB)[40–42], which is responsible not only for conformation of the dimer but also for elongation of C1-N2 bond while bonds within N2-C2-N3 fragment retains π-conjugated.

When two molar equivalents of appropriate lithium amide are added to the 1,2-dicyanobenzene, only the mixture of Li**1a**, Li**1b** or Li**1d** together with unreacted amides were obtained, which supports the fact that no further addition reactions to the silylated lithium DIIs are possible at specified conditions. Unfortunately, these reactions cannot be performed at elevated temperature as the starting amides are instable in coordinating solvents above 40°C.

In addition, the microwave treatment of the reaction mixture after the water treatment of Li**1a** in xylenes yields the product of DII condensation and subsequent coordination of lithium atom – Li**2a** (Scheme 2). In this dinuclear centrosymmetric structure, the lithium atom is bound by one DII inside the six-membered heterocyclic ring and by second DII via exocyclic nitrogen atom. Oxygen atom of the diethyl ether molecule (recrystallization solvent), as a center of symmetry, is coordinated to both lithium atoms. Similar DII fragment can be also prepared by heating neat compound **1b** to 180 °C. Upon heating, elimination of ammonia occurs and self-condensation product **2b** consisting of two DII units is formed (inseparable mixture with **1b**) (Scheme 2., see SI Figs. S46– S47 and S52 for more details and crystal structures).

On the other hand, when we repeated the preparation of the complex Li**1b**, significant amount of air and moisture was accidentally allowed to penetrate into the reaction vessel after a couple of minutes of the reaction. It seems, moisture destroyed unreacted portion of lithium amide and thus the 1,2-dicyanobenzene became slightly excessive. Unknown type of lithium complex Li**3b'** as partially hydrolyzed product of the addition of Li**1b** to 1,2-dicyanobenzene was isolated as orange crystals and characterized in solution as well as in the solid state (Scheme 4, see SI Fig. S49).

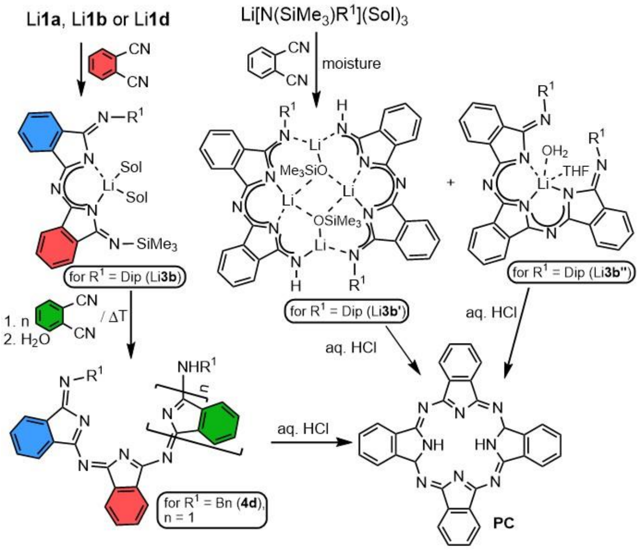

Scheme 4. Observed reactivity of silylated lithium DIIs; Dmp = 2,6-dimethylphenyl-; Dip = 2,6-diisopropylphenyl-; Sol = THF, diethyl ether.

Obviously the second bis(imino)isoindoline moiety was created via further migration of the trimethysilyl group, which is essential for the second addition. This has been also documented by the fact the diiminoisoindoline **1b** does not provide any product containing two bis(imino)isoindoline units, when deprotonated by lithium diisopropylamide, treated with 1,2-dicyanobenzene and subsequently hydrolyzed. Li**3b'** consists of dimeric arrangement of slightly deformed planar heterocyclic units interconnected by four lithium atoms where two of them compensate negative charge of each of the ligands and the second two came from the product of the partial hydrolysis of the complex - the lithium trimethylsilanolate. The first two are found in plane of the ligand completing the central six-membered ring together with exocyclic nitrogen atoms, the second couple of lithium atoms is located at peripheries complexed by endocyclic nitrogen atoms below and above the central ring by ca 0.66 Å. Lithium atoms in the central area are four coordinated in the vicinity of distorted tetrahedra while the peripheral ones have trigonal planar geometry and both are connected by the trimethylsilylanolate units. The only deprotonable hydrogen atom is localized on the peripheral imino nitrogen on the opposite side to the Dip group. Very minor species Li**3b''**, characterized exclusively by sc-XRD methods, arose as a byproduct of that reaction alongside Li**3b'** (Scheme 4., see SI S49). Complex Li**3b''** consists of three interconnected DII units, where the terminal nitrogen atoms are substituted by Dip groups (Fig. S50). All three isoindole nitrogen atoms of that monoanionic ligand coordinate the lithium atom in a planar fashion similarly as the four DII units in neutral lithium phtalocyanines[43]. Further donors to lithium ion in Li**3b''** are THF and water molecule, which forms H-bonds to peripheral imino groups. For all the compounds with more than one DII unit, the terminal imino groups *E*-isomers were observed in the solid state and one can also suggest the same arrangement in solution. By acidolysis of Li**3b'** and Li**3b''** by aqueous HCl, new unprecedented pathway to phthalocyanine **PC** (characterized by IR spectroscopy and Mass spectrometry – Figs. S140 and S145) is available (Scheme 4). Plausible mechanism of this reaction can be similar to various sequential mechanisms initiated and templated by metals reported earlier.[44]

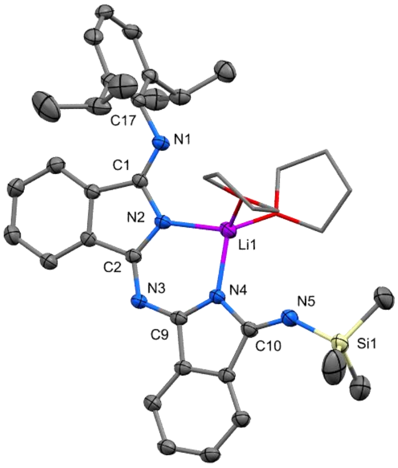

Figure 4. The molecular structure of Li**3b**, ORTEP view 50% probability level. Hydrogen atoms are omitted for clarity. Selected bond lengths (Å) and angles (°): N1–C17 1.427(4), N1–C1 1.273(3), C1–N2 1.414(4), N2–C2 1.332(3), C2–N3 1.343(3), N3–C9 1.349(4), N4–C9 1.330(3), N4–C10 1.422(4), N5–C10 1.270(3), N5–Si1 1.732(3), N2–Li1 2.019(5), N4–Li1 1.985(5), C1–N1–C17 121.8(2), N1–C1–C4 131.1(2), N2–Li1–N4 90.0(2), C10–N5–Si1 138.7(2).

Characterization of Li**3b'** led us to the idea to prepare a lithium complex containing the trimethylsilyl and Dip group connected to the moiety composed of two diiminoisoindoline fragments. The excess of 1,2-dicyanobenzene (two molar equivalents) was added to solutions of the parent amides. After the conversion of the amide Li[N(SiMe$_3$)Dip](THF)$_3$, two types of crystals were isolated from the solution - minor number of green-yellow ones determined to be Li**1b** and orange crystals of Li**3b**. Complex Li**3b** (Fig. 4), as expected, containing two diiminoisoindoline fragments as well as Dip and SiMe$_3$ substituent on exocyclic nitrogen atoms. This complex is mononuclear, and lithium atom is coordinated by two isoindole nitrogen atoms in planar arrangement, furthermore two donor THF molecules are present.

Insoluble green, presumably oligomeric material **4d**, has been isolated when an excess of 1,2-dicyanobenzene was added to Li**1d** or Li**3d** (Scheme 4), warmed to 50 °C for four hours, and poured into cold water. This procedure was followed by filtration and Soxhlet extraction of both solid samples by dichloromethane in order to remove unreacted material 1,2-dicyanobenzene and substituted DIIs with lower molar masses. Crude products treated by water or HCl gave deep blue crystalline material. The extracts were subjected to HR-MS spectrometry investigation. In the deep blue sample, prepared at acidic conditions, almost pure unsubstituted phthalocyanine (**PC** - Pigment Blue 16) was identified by mass of 515.1727 Da and identical IR spectrum. The treatment at neutral conditions gave a petrol green sample, mixture of compounds consisting of two or three DII units and benzyl substituent, characterized by exact masses of 582.2408, 492.1936, and 364.1563 Da and molecular formulae $C_{38}H_{28}N_7$, $C_{31}H_{22}N_7$ and $C_{23}H_{18}N_5$, respectively. Further treatment of green sample by aqueous HCl gave immediately blue solid, identical by spectral analysis to **PC** from the first procedure.

DII-guanidines: Synthesis, structure and tautomerism investigation

To the best of our knowledge, there is a limited number of species where the direct connection of DII and guanidine fragments is present. The first class of these organic compounds and metal (Re, Mn, Cu, Fe) complexes is characterized by middle DII group symmetrically *N*-substituted by another diiminoisoindoyl fragments with a planar structure of terdentate ligand for Mn, Cu and Fe[45–48]. While the second class are DIIs substituted by two pyridin-2-yl or pyrimidin-2-yl fragments are used as *C*,*N*,*N*- or *N*,*N*,*N*-chelating ligands for palladium[49] or as preorganized ion traps[49]. Both compounds **1a** and **1b** exhibit an activated nature of NH or NH$_2$ functional groups in sense of very good performance in the nucleophilic addition to cumulated unsaturated system of carbodiimides, which is simple for aliphatic amines and/or carbodiimides[51, 52]. On the other hand, the synthesis of guanidines bearing aromatic or bulky substituents usually need harsh conditions or metal catalysis[53–56]. DII-guanidines **5aa**–**5bb** (Scheme 5) were prepared in very good yields in warm toluene without any catalyst in 48 hours. Chemical structure of **5aa**–**5bb** in solution was investigated by NMR spectroscopy.

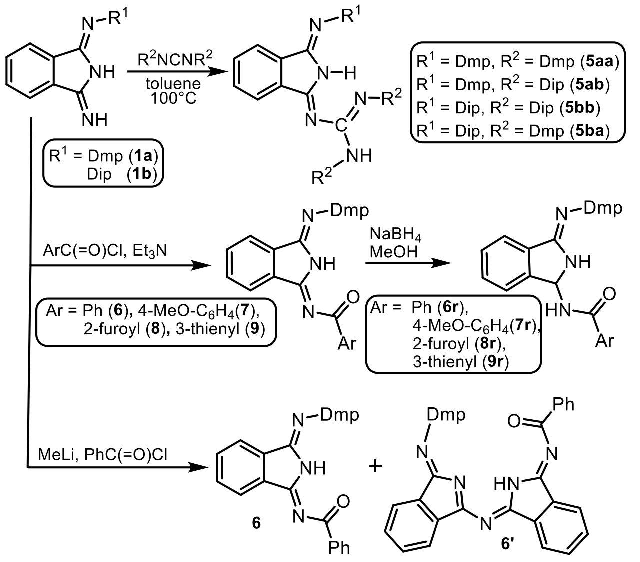

Scheme 5. Derivatization of DIIs **1a** and **1b**.

NMR spectroscopy revealed significant solvent effect in all four compounds **5aa**–**5bb**. While in C_6D_6, two sets of signals in 95:5 ratio were observed, in THF-*d$_8$* the only one set of NMR signals indicating just one stable form, was found. ^{1}H spectra of all compounds in this series revealed one down-field shifted signal of NH involved in strong intramolecular hydrogen bond (12.56 ppm for **5ab** as an illustrative example – see Fig. 5B). There are two hypothetical tautomers fulfilling criterion for a strong RAHB, with hydrogen atom attached to N2 or N5 atoms (Fig. 5). Position of NH could be assigned by ^{1}H, ^{13}C-HMBC NMR experiment. However, HMBC revealed spin-spin interaction of NH with carbon atoms from the indole part as well as from the phenyl part as shown in Fig. 5. This indicates possible co-existence of both tautomers. To inspect this, we measured NMR spectra at low temperature (-100 °C), but no additional set of signals were detected. Therefore, the tautomeric equilibrium must be investigated by an advanced NMR approach including quantum-chemical calculations.

When investigating tautomeric equilibria of small molecules, experimentally obtained NMR parameters are systematically correlated with the calculated values of each particular tautomer. First, geometry of all possible tautomers is optimized, and from the low-energy forms the NMR parameters are calculated. Usually, ^{13}C chemical shifts are used for study of tautomeric equilibria. However, we obtained all the correlations with correlation factor $R^2 > 0.99$ (Figures S4 – S10 in SI), precluding unambiguous determination of the present tautomeric forms. With respect to the fact that guanidines are rich of nitrogen atoms, we decided to use ^{15}N NMR parameters for our investigation. Although the natural abundance of ^{15}N is low (0.4%), we succeeded in extraction of ^{15}N chemical shifts from 2D -^{1}H, ^{15}N NMR experiments. Moreover, five nitrogen atoms in the molecule is a sufficient number for construction of linear regression needed for correlation of experimental data with the calculations. As an example, we show tautomeric equilibria of compound **5ab (Fig. 5)**. In **5ab**, ^{15}N NMR/DFT correlations of 2,4-tautomer showed R^2 0.5414, on the other hand, R^2 for N5 tautomer was

0.9640 (Figures S11 – S14 in SI). The calculated data did not match the experiment perfectly. Furthermore, the energy difference between 2,4- and 4,5-tautomers was estimated to be 0.46 kcal/mol corresponding to ca. 7:3 ratio with 4,5-tautomer to be a predominant form. Averaging the calculated ^{15}N shielding constants according to Boltzmann distribution provided the best fit $R^2 = 0.9981$ (Fig. 5). Based on these results, we believe that in solution is a tautomeric equilibrium where 70% of 4,5-tautomer is present. The same approach was applied to the rest of the compounds from this series as shown in Section Figs. S11 – S14 in SI.

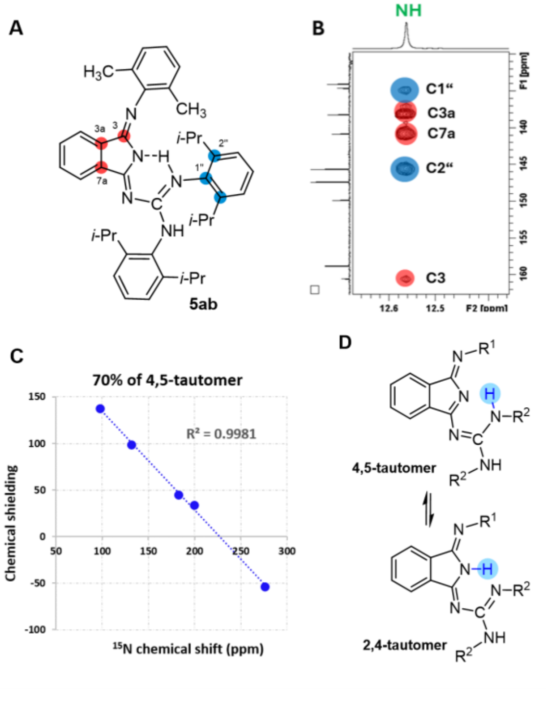

Figure 5. (A) Structure of compound **5ab**. (B) A part of HMBC of **5ab** showing that NH involved in intramolecular hydrogen bond (12.56 ppm) provides crosspeaks corresponding to spin-spin interaction through 2 and 3 chemical bonds to both moieties indicating tautomeric equilibrium. (C) ^{15}N NMR/DFT correlation of **5ab**. ^{15}N NMR were measured in THF-*d₈* at 25 °C, the geometry was optimized at B3LYP/6-31g(d,p)/PCM(THF) level of theory and the NMR parameters were calculated at B3LYP/6-311+g(d,p) PCM(THF) level of theory. (D) Possible tautomeric equilibrium.

The tautomeric equilibria of **5aa**–**5bb** were also investigated in solid state by XRD. With respect to the maxima attributable to the N-H atoms on the Fourier difference electron density maps the hydrogen atoms were placed on N5 atom of guanidine in cases of **5aa** and **5ab**, and to the N2 atom of the DII moiety in cases of **5ba** and **5bb**, respectively. This placement is in line with the description of bonding situation within the central DII-guanidine moiety and the concept of conjugation of π-electron density. On the other hand, we are aware of alternative descriptions operating with the mixture of both discrete tautomers in the solid state and as such with a placement of hydrogen atom to both positions with partial occupancy as first described by Bertolasi and Gilli[57].

Although all the **5aa**–**5bb** have very close molecular structures one to each other, some discrepancies are observable. Predictably, the compounds with smaller Dmp substituents, especially at the DII fragment are a bit more compact with nearly ideal planar arrangement of the DII and guanidine groups, thus forming the structure with characteristic six-membered ring N=C—N=C—N(H) connected by relatively strong H-bond. Presence of the Dip groups in the molecules causes a non-negligible distortion of the N5 atom from the plane defined by DII and C3 atom of the guanidine part (see SI Fig. S58). Differences between structures of **5aa**–**5bb** are also seen when careful comparison of the interatomic distances inside the DII and guanidine fragment is made. For compounds **5aa** and **5ab** is the most representative 4,5-tautomer containing both hydrogen atoms on guanidine unit (Fig. 6). Bond distribution consists of localized set of single and double bonds C9-N1-C1-N2 and then delocalized system within N-C-N guanidine fragment. Compounds **5ba** and **5bb** are represented as 2,4-tautomers, with one hydrogen atom located on isoindole and the second one on guanidine fragment (Fig. 6). Taking into the account atom separations within whole molecules of both tautomers, major differences are found in the guanidine fragments. Guanidines in 2,4-tautomers of **5ba** and **5bb** exhibit a higher localization of π-electron density. Depending on substituent, interatomic distances within guanidine are prolonged due to effect of steric hindrance.

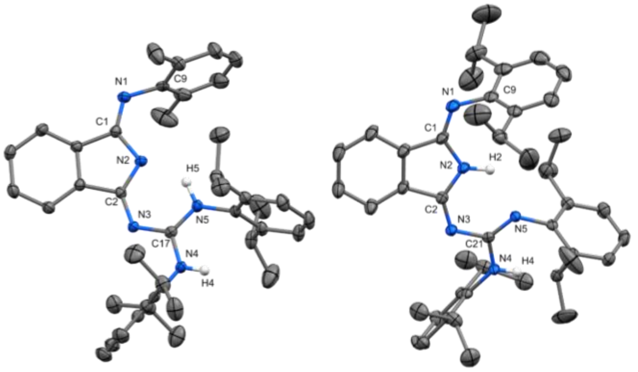

Figure 6. The molecular structures of **5ab** (left) and **5bb** (right), ORTEP views 50% probability level. Hydrogen atoms are omitted for clarity. Selected bond lengths (Å) and angles (°) for **5ab**: N1–C9 1.4216(17), N1–C1 1.2753(16), C1–N2 1.4055(15), N2–C2 1.3467(15), C2–N3 1.3249(15), N3–C17 1.3573(15), N4–C17 1.3556(15), N5–C17 1.3278(16), C1–N1–C9 119.95(11), N1–C1–C4 124.69(11), C2–N3–C17 119.42(10), N4–C17–N5 119.96(11). For **5bb**: N1–C9 1.419(2), N1–C1 1.271(2), C1–N2 1.4085(18), N2–C2 1.361(2), C2–N3 1.3013(18), N3–C21 1.3573(15), N4–C21 1.3880(18), N5–C21 1.3005(19), C1–N1–C9 121.07(13), N1–C1–C4 125.30(13), C2–N3–C21 118.88(13), N4–C21–N5 122.16(12).

With the aim to use compounds **5aa**–**5bb** as protoligands in coordination chemistry, their reactivity with *n*-BuLi, LDA and MeLi was explored to find most efficient deprotonating agent. One molar equivalent of *n*-BuLi and MeLi did not provide quantitative deprotonation in case of **5aa**–**5bb**. However, one equivalent of LDA performs deprotonation of the most acidic hydrogen atom in **5aa** and **5ab** quantitatively. For sterically more hindered compounds **5ba** and **5bb**, conversions of analogous reactions are only around 46% and can be increased by addition of an excess of LDA, unfortunately the quantitative conversion has never been achieved (see SI Table S10.).

Amido derivatives: Synthesis, structure, E/Z-isomerization and dimerization investigation

As the next target, the DII **1a** substituted by an acyl moiety was selected. The major motivation was to establish novel type of species with DII unit and the carbonyl group in the structure, which would be capable to coordinate metal center. The only example of similar species is found in attempted synthesis of novel type of helical structure[58]. The major idea is based on the formation of compounds with two substituted DII fragments bridged by 2,6-pyridinedicarbonyl. Instead of tautomeric form necessary for the formation of suggested intramolecular H-bridge, different arrangement was observed.

Proposed synthetic procedure can be based on direct reaction of silylated DII Li**1a** (Scheme 2) or **1a** with an acyl chloride in a presence of a base. We have chosen the second pathway, which would presumably give lower number of byproducts. The selected procedure took into the account the problems connected to high steric hindrance of Dip-substituted species and thus lower efficiency of deprotonation process described above for DII-guanidine compounds.

First, we used **1a** and deprotonated it in situ by MeLi followed by an addition of acyl chlorides (Scheme 5). Surprisingly enough, only two types of acyl-substituted DIIs were formed according to the NMR monitoring. Separation of these types of compounds by crystallization of reaction mixtures gave yellow crystals of desired species **6**–**9** in about 85 to 90% yields. For the red crystals, which can be separated from the yellow ones only mechanically. The identification is based on further NMR studies and crystal structure determination of phenyl substituted compounds **6** and **6'** having two interconnected DII units as described below. The formation of these minor species is precluded by using the second procedure, addition of triethyl amine to the mixture of **1a** with acyl chlorides. ^{1}H NMR spectra of all analytically pure **6**–**9** provided two sets of signals in 2:1 ratio indicating two distinct forms. ^{1}H spectrum combined with ^{1}H,^{15}N-HSQC showed that each form has one NH group with the hydrogen atom involved in strong intramolecular hydrogen bond indicated by down-filed shifted signals (10.5 ppm for major form and 11.2 ppm for the minor form). The careful analysis of ^{1}H spectra uncovered the biggest chemical shift difference between both forms at H4 hydrogen atom (Δδ 1.5 ppm) and ^{15}N chemical shift of NH nitrogen atom differing of more than 6 ppm (see SI Fig. S45). This indicates sterically hindered rotation/inversion at C1-N1 bond (Fig. 8), which can be further investigated by variable-temperature NMR. The ^{1}H spectra measured at 60 °C showed significant signal broadening of H4 signal compared to H7 (Fig. 7).

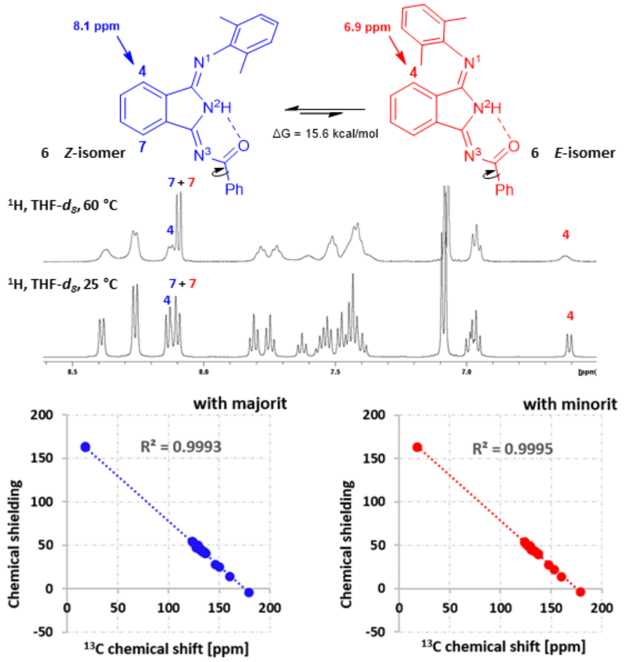

Figure 7. The proposed *E*/*Z* isomerization of **6**. Variable-temperature ^{1}H NMR spectra of **6** showing significant signal broadening of H4 compared to H7 at 60 °C. ^{13}C NMR/DFT correlation of **6**. ^{13}C NMR were measured in THF-d_8 at 25 °C, the geometry was optimized at B3LYP/6-31g(d,p) / PCM(THF) level of theory and the NMR parameters were calculated at B3LYP/6-311+g(d,p) PCM(THF) level of theory.

This supports our hypothesis about a co-existence of two isomers differing in orientation of dimethyl phenyl moiety (*E*/*Z*). Moreover, H4 of the major form (*Z*-isomer) is less shielded (higher chemical shift) than the same atom in the minor form - *E*-isomer. This makes H4 signal a diagnostic for molecular geometry evaluation in solution, which may be useful for more structurally complex molecular systems such as metal complexes. To support our experimental results, we employed DFT calculations to all studied derivatives **6**–**9**. From the optimized structures of each isomer, NMR parameters were calculated. ^{13}C shielding constants of each particular isomer were correlated with the experimentally obtained ^{13}C chemical shifts. Calculated ^{13}C shielding constants of *Z*-isomer nicely matched with the set of signals for more populated form, simultaneously, *E*-isomer fits with the set of minor signals ($R^2 > 0.999$, details in SI). Calculated transition-state structures and the free energy barrier ΔG^{TS} were estimated to be around 15.5 kcal/mol for all derivatives, the OMe derivative **7** displayed the highest barrier of 15.8 kcal/mol (details in SI Fig. S15 – S38). These values are reasonable and support our hypothesis that the two forms are correctly identified as *E*/*Z* isomers. In turn, we have also calculated ΔG^{TS} of flipping the coplanar heterocyclic ring of **8** and **9** (depicted by circular arrows in Fig. 7), which was estimated to be 11.5 and 9.2 kcal/mol, respectively. Such a low ΔG^{TS} cannot result in two distinct sets of NMR signals even at low temperature.

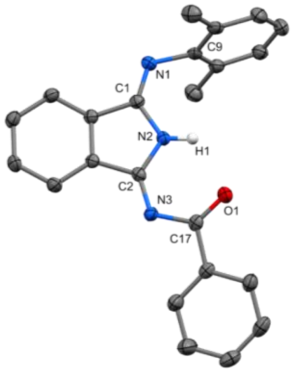

Figure 8. The ORTEP view 50% probability level of molecular structure of **6**. Hydrogen atoms are omitted for clarity. Selected bond lengths (Å) and angles (°): N1–C9 1.427(2), N1–C1 1.267(2), C1–N2 1.407(2), N2–C2 1.368(2), C2–N3 1.296(2), N3–C17 1.392(2), O1–C17 1.227(2), C1–N1–C9 120.28(16), N1–C1–C4 126.08(17), C2–N3–C17 118.77(15), N3–C17–O1 125.08(17).

In the solid state, all the structures of **6**–**9** (for illustration see **6** in Fig. 8) exhibit perpendicular arrangement of Dmp substituent to the planar molecular structure of isoindole core. Acyl substituents in compounds **7**–**9** are in planar arrangement with isoindole core too, while substituent in compound **6** exhibits deviation from the plane by ca 18°. Within their structure, five-membered N-C=N-C=O arrangement is formed and allows an ideal neighborhood for metal coordination. The direct comparison of that structures with **1a**–**5bb** shows differences in bond distribution and hydrogen localization. Compounds **6**–**9** contain discrete system of single and double bonds without any delocalization or polarization influence. Hydrogen atom is undoubtedly found at the endocyclic nitrogen of DII and is involved in very short resonance-assisted H-bond with oxygen atom from acyl substituent. In case of structures **8** and **9** is furthermore possible to observe static disorder caused by a flip of furoyl or thienyl substituent similarly as predicted by DFT (*vide supra*).

Minor product **6'** of the reaction between **1a**, deprotonated by MeLi, and benzoyl chloride (Scheme 5) was characterized in the solid state. It consists of two DII fragments with Dmp and acyl substituent on exocyclic nitrogens (Fig. 10). Dmp substituent is in perpendicular arrangement to DII dimeric planar structure and acyl substituent, similarly to compound **6**, is deviated from the plane by about 30°. Hydrogen is located on endocyclic nitrogen N4 near the acyl substituent, which allows formation of intramolecular hydrogen bond with oxygen atom. The second hydrogen bond takes place as well, this time with endocyclic isoindole nitrogen N2. Compound **6’** as well as **6**–**9** contain localized system of single and double bonds. With a closer look, a formation of **6’** is not that simple and consists of several steps (Fig. 9). This side reaction of the preparation of **6** by MeLi procedure is allowed only by equilibria between **1b** and its mono- and dilithiated forms during the synthesis. Twice deprotonated dilithiated complex reacts with benzoyl chloride to compound Li**6’** with two fused DII moieties. Li**6’** exists in solution in the form of two monolithiated isomers, where the lithium atom is coordinated by two solvent molecules (THF or water). Both *E*- and *Z*-isomers coexist in nearly equimolar ratio (Fig. 9) after the reaction under inert conditions in THF-d_8, presumably as bis-tetrahydrofuranates. In CD_2Cl_2 only the *E*-isomer exists. Both isomers of Li**6’** exhibit almost the same diffusion coefficients in both DOSY NMR spectra, recorded in CD_2Cl_2 and THF-d_8, corresponding to a monomeric behavior (see SI Fig. S43–S44). When the complex is crystallized from diethyl ether on air, the dimer (Li**6’**)$_2$·H_2O connected by one water molecule crystallizes out of the solution (see SI Fig. S70). Both pairs of connected DII-DII units exhibit the *E*-isomer structure with Dmp group nearly (89.02(9)°) perpendicularly oriented towards them. The interplanar angle between DII-DII parts is 62.08(12)°, while the benzoyl groups are a bit deviated from the major plane (25.82(11)°). The lithium atoms are found in centers of pseudo square pyramidal vicinity formed by ligands in a terdentate fashion and with carbonyl groups in the bridging apical position. Bridging water molecule is found in the basement of the polyhedra. In contrast to compound **6’** as well as **6-9**, structure of compound Li**6’** contains extensive delocalized bond system from N2 to C25 (see SI Fig. S70), as a result of lithium atom coordination.

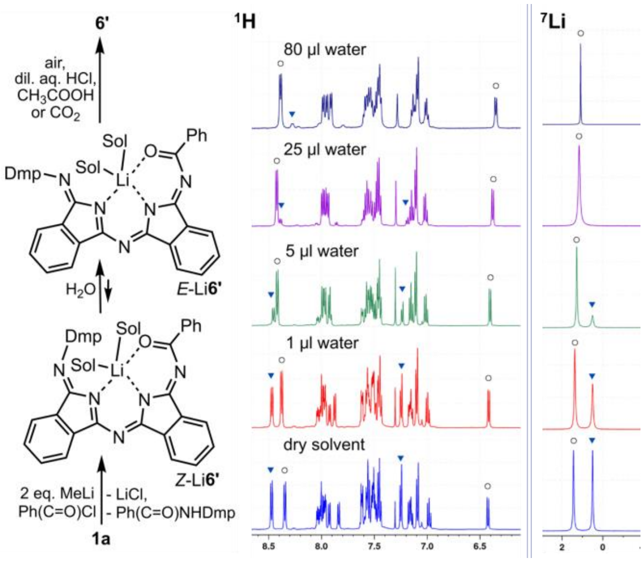

Figure 9. Side reaction of benzoyl derivatization of **1a** - left. ^1H (middle) and ^7Li (right) NMR spectra of the equilibrium between *Z*-Li**6’** and *E*-Li**6’** influenced by gradual addition of water.

The equilibrium of Li**6’** was monitored by ^1H and ^7Li NMR spectroscopy in THF-d_8 solution (Fig. 9, see SI S39 – S40). At the beginning, the *E*- and *Z*-isomers are present in 1:1 ratio, but upon opening of the tube to the air and gradual addition of water, the equilibrium is shifted significantly towards the *E*-isomer characterized by the diagnostic signal of H4 atom (δ=6.4), similarly as for **6** (Fig. 8). When the sample is left on the air or treated with diluted aqueous HCl, CH_3COOH or CO_2, as a weak acid, is bubbled through the sample (see Fig. 9), lithium and solvents are extruded from the structure of Li**6’**, forming the *Z*-isomer of **6’** in the solid state (Fig. 10). Both possible isomers were detected in CD_2Cl_2 or THF-d_8 solutions with more populated *Z*-isomer in ratio of 2:1 and 5:1, respectively.

Amido derivatives: reduction

As the last topic, we explored a novel synthetic route to amido derivatives of reduced DIIs, which can be seen as possible precursors of hemiporphyrazines, valuable species with new metal complexation patterns, fluorescent dyes or 2D materials[59–61]. Simple reduction of **6**–**9** (Scheme 5) by sodium borohydride in methanol gives after recrystallization from diethyl ether **6r**–**9r** in the form of etherates. Diethyl ether can be easily removed from the solid samples by dynamic vacuo. Formal hydrogenation takes place at the imino group of the diiminoisoindole instead of the amide reduction. The ability of these compounds to make an intramolecular H-bonds is suspended by the reduction of π-electron density and the C2 atom became sp^3 hybridized. Also, the *E*/*Z* isomerism and tautomeric exchanges observed in previously described compounds are expected to be vanished. It is worth to be mentioned **6r**–**9r** were prepared as racemic mixtures with chiral center at C2 atom.

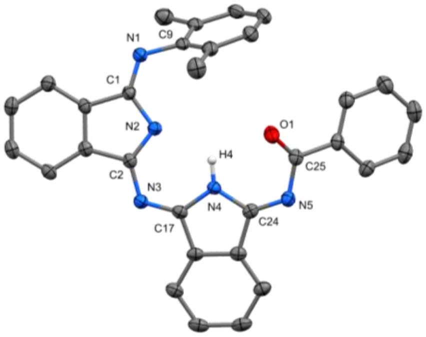

Figure 10. The ORTEP view 50% probability level of molecular structure of **6’**. Hydrogen atoms are omitted for clarity. Selected bond lengths (Å) and angles (°): N1–C9 1.4211(18), N1–C1 1.272(2), C1–N2 1.4219(19), N2–C2 1.3168(18), C2–N3 1.373(2), N3–C17 1.2985(19), N4–C17 1.3810(17), N4–C24 1.3908(19), N5–C24 1.2863(18), N5–C25 1.399(2), O1–C25 1.2237(18), C1–N1–C9 121.13(13), N1–C1–C4 123.26(14), C2–N3–C17 119.97(12), C24–N5–C25 119.15(13).

NMR analysis of **6r**–**9r** showed only one set of signals clearly determining the proposed structures. By the reduction, the pyrrole ring lost the key double bond needed for π-electron conjugation of both neighboring imino groups, which also led to discontinuation of the RAHB and non-existence of any other intramolecular hydrogen bond. This is clearly reflected in ^1H NMR spectrum, where the NH signal of H2 atom is shifted from ca 10 ppm to 6.7 ppm (in the case of **6r**). The loss of aromaticity is also demonstrated by a loss of color.

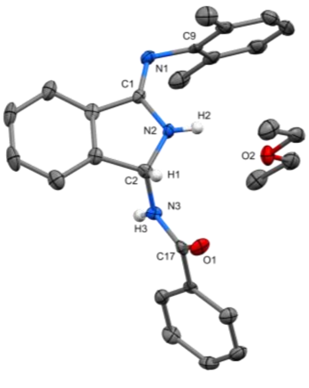

Figure 11. The ORTEP view 50% probability level of molecular structure of **6r**. Hydrogen atoms are omitted for clarity. Selected bond lengths (Å) and angles (°): N1–C9 1.421(6), N1–C1 1.280(6), C1–N2 1.359(6), N2–C2 1.455(6), C2–N3 1.450(6), N3–C17 1.346(6), O1–

C17 1.237(5), C1–N1–C9 117.0(4), N1–C1–C4 124.4(4), C2–N3–C17 122.7(4), N3–C17–O1 121.9(4).

In the solid state, all the compounds of this series are prone to crystallize (Figs. S66–S69) in the same achiral space group *Pna*2$_1$. The planarity of the reduced DII fragment retained almost ideal. The Dmp substituent is oriented perpendicularly as described for less saturated **6**–**9**. However, position of the acyl substituent is significantly different and its deflection from the DII plane is approximately 84°. Bond lengths distribution differs (see Fig. 11) when compared to the rest of substituted DIIs, and as direct consequence of chemical reduction, interatomic distances in N2-C2-N3 fragment are elongated. Hydrogen bond is no longer intramolecular, but between N3-H3 group and carbonyl oxygen atom from another DII molecule occurs the infinite chain (peptide-like) intermolecular hydrogen bond. The NH groups of DIIs are saturated by an H-bond electron transfer from oxygen atom of diethyl ether solvate.

CONCLUSIONS

As a contribution to the chemistry of macrocycles and reactivity of lithium amides with unsaturated systems, this work opens new pathway to synthesis of dissymmetrically substituted DIIs. These can be used as precursors to a large variety of phthalocyanines with variable structures. Novel types of organic compounds with preorganized structures usable as starting materials for construction of hemiporphyrazines and similar macrocyclic compounds have been investigated. Several types of isomerisms in solution have been studied by NMR/DFT approach - *E*/*Z*-isomerization and dimerization (DII **1a** and amido derivatives **6**–**9**), tautomerism (guanidines **5aa**–**5bb**) and stability both in solution as well as in solid state. This could help the selection of appropriate precursor or ligand, solvent and conditions when targeted applications will be quested, which is further documented by synthesis of appropriate lithium complexes. The presence of strong resonance-assisted hydrogen bonds in series of compounds **1a**–**1e**, **2b**, **5aa**–**5bb**, **6**–**9** predetermined their use as novel ligands for coordination chemistry similarly as acetylacetonates or β-diketiminates.

MATERIALS AND METHODS

Synthesis

Multiple manipulations and reactions were carried out under an argon atmosphere using standard Schlenk techniques (stated in experimental procedures). Reagents were purchased from commercial suppliers (Merck or Avantor/VWR) or were already available at our labs. The solvents were dried and degassed using PureSolv^{TM} solvent drying system (Innovative Technology Inc., USA). For detailed description see Supporting Information.

*General procedure for synthesis of compounds Li**1a**, Li**1b**, Li**1c**, Li**1d** and Li**1e***

Aniline was dissolved in hexane, and *n*-butyllithium was added at 0 °C. The yellow solution was stirred for another hour, concentrated in vacuo, and the yellow crystalline intermediate was isolated. Intermediate was dissolved in THF and a solution of 1,2-dicyanobenzene in THF was added while cooling to -50°C. A dark green solution was formed, which was left to stir for 12 hours and subsequently, at a low temperature (-20°C), the product was recrystallized from THF or a mixture of THF and petroleum ether. The product was filtered off, washed twice with hexane, and dried in vacuo. Reactions were performed under an argon atmosphere using standard Schlenk techniques.

General procedure for synthesis of compounds **1a**, **1b** and **1c**

Lithium complex was dissolved in methanol on air, and two molar equivalents of water were added. The solution was left to stir for 12 hours and then the solvent was evaporated under vacuo. The product was extracted by dichloromethane, filtrated, dried in vacuo and isolated in the form of a yellow powder.

*General procedure for the synthesis of compounds **5aa** – **5bb***

The corresponding isoindole was dissolved in 30 mL of toluene at 50 °C. Subsequently, one molar equivalent of carbodiimide was added to the solution. The reaction mixture was stirred for 48 hours at 100 °C, then cooled to room temperature and concentrated in vacuo. The product was further washed with hexane, dried and isolated as a yellow powder.

*General procedures for synthesis compounds **6** – **9***

Procedure A

The corresponding isoindole was dissolved in 30 mL of diethylether. The solution was cooled to 0 °C, and one molar equivalent of methyllithium was added. The reaction mixture was stirred for 1 hour at room temperature. Subsequently, one molar equivalent of acyl chloride was added to the solution. The solution was stirred for 4 hours with the formation of a yellow precipitate, then concentrated in vacuo to half. The product was filtrated from a solution and extracted with benzene. After evaporation of benzene in vacuo the product was dried and isolated as a yellow powder. The reactions were carried out under an argon atmosphere using standard Schlenk techniques.

Procedure B

Corresponding isoindole was dissolved in 50 mL of diethylether. Subsequently, one molar equivalent of acyl chloride and two equivalents of triethylamine were added to the solution. Solution was stirred for 12 hours and filtrated on a frit. Product was gained from solution by slow evaporation of diethyl ether. After filtration the product was dried and isolated as yellow crystals.

*General procedure for reduction compounds **6** – **9***

To a mixture of isoindole and sodium tetraborohydride hexane was added, the suspension was cooled down to -30 °C and 0.250 mL of methanol were added. The solution was left to stir for 2 hours. Then the solution was filtrated from a highly viscous by-product and the solvent was evaporated under vacuo. The product was dried in vacuo and isolated in the form of a pale-yellow powder. Reactions were carried out under an argon atmosphere using standard Schlenk techniques.

NMR spectroscopy

NMR experiments were performed on a Bruker Avance III spectrometer equipped with a broad-band cryo probe with an ATM module (5 mm CPBBO BB-^{1}H/^{19}F/^{15}N/D Z-GRD) operating at 499.98 MHz for ^{1}H, 125.73 MHz for ^{13}C and 50.67 for ^{15}N; and also on a Bruker Avance III 600 spectrometer equipped with an inverse triple resonance cryoprobe with ATM module (5 mm CPTCI 1H/13C/15N/D Z-GRD) operating at 600.13 MHz for ^{1}H and 60.82 MHz for ^{15}N. Low-temperature NMR spectra were recorded on a Bruker Avance II spectrometer with a triple resonance broad-band probe with ATM (5 mm PATBO BB−1H/19F/D Z-GRD) operating at 499.94 MHz for ^{1}H and 125.72 MHz for ^{13}C. For NMR signal assignment, standard Bruker pulse sequences were employed for both 1D (^{1}H, ^{13}C-APT) and 2D (COSY, ROESY, HSQC, HMBC) NMR experiments at a corrected temperature. All NMR data was interpreted using Topspin 3.5. For reference, the following solvent signals were used: DMSO-d_6: 2.50 (^{1}H) and 39.5 (^{13}C) ppm; THF-d_8: 3.57 (^{1}H) and 67.57 (^{13}C) ppm, toluene-d_8: 2.08 (^{1}H) and 20.43 (^{13}C) ppm. The solutions were obtained by dissolving approximately 20 mg of each compound in 0.6 mL of the deuterated solvent.

The DOSY spectra were acquired in 5 mm NMR tubes and all the experiments were performed at 25°C and without sample spinning to avoid convection. All DOSY experiments were performed using standard Bruker pulse sequence - dstebpgp3s - a double stimulated echo sequence with bipolar gradient pulses and three spoil gradients with convection compensation. The diffusion time was 0.1 s (D). The duration of the magnetic field pulse gradients was adjusted for each polymer in a range of 500–2000 ms (d/2). The delay for gradient recovery was 0.2 ms and the eddy current delay 5 ms. For each DOSY-NMR experiment, a series of 16 spectra on 32 K data points were collected. The pulse gradients were incremented from 2% to 98% of the maximum gradient strength in a linear ramp with a total experiment time of 23 min. The temperature was set and controlled at 295 K with an air flow of 400 L/h in order to avoid any temperature fluctuations due to sample heating during the magnetic field pulse gradients. After Fourier transformation and baseline correction, the diffusion dimension was processed with the Topspin 3.6.1 software and Dynamic Center 2.4.4.

Mass spectrometry

High resolution EI spectra were measured using Agilent 7250 GC/Q-TOF mass spectrometer (Agilent). The conditions were optimized for suitable ionization in the source (electron voltage 70V, source temperature 230 °C). The sample was applied either by direct injection or using attached GC module (column DB-5, 30 m; flow rate of helium 1 ml/min).

High resolution ESI spectra were measured using LTQ Orbitrap XL (Thermo Fisher Scientific). The conditions were optimized for suitable ionization in the source (capillary voltage 9V, tube lens voltage 150V, temperature 275 °C). The sample was applied by direct injection in positive and the mobile phase was 80% MeOH with the same flow rate.

sc-XRD

Full-sets of diffraction data were collected at 150(2)K with a Bruker D8-Venture diffractometer equipped with Cu (Cu/*K*α radiation; λ =1.54178 Å) or Mo (Mo/*K*α radiation; λ = 0.71073 Å) microfocus X-ray (IμS) source, Photon I or III CMOS detectors and Oxford Cryosystems cooling device was used for data collection. Some data were collected at the same conditions at Nonius KappaCCD diffractometer with MoK_{α} radiation (λ = 0.71073 Å), a graphite monochromator, and the ϕ and χ scan mode. The frames were integrated with the Bruker SAINT software package using a narrow frame algorithm. Data were corrected for absorption effects using the Multi-Scan method (SADABS).[62] Obtained data were treated by XT-versions 2014/5, SHELXT 2018/2[63] and SHELXL-2018/3 software[64] implemented in APEX3 / APEX4 (Bruker AXS) system.[65] The hydrogen atoms were placed in calculated positions and refined in the “riding model”. Some H atoms were localized on a difference Fourier map. Heavy atoms were refined anisotropically. Hydrogen atoms were mostly located on the difference Fourier map, however, for the final solution of the crystal structure, all hydrogen atoms were recalculated into ideal positions (riding model) according to the assigned temperature factors $H_{iso}(H) = 1.2\ U_{eq}$ for aryl groups and $H_{iso}(H) = 1.5Ueq$ for aliphatic groups with C-H bond lengths = 0.96; 0.97; 0.98 and 0.93 Å for methyl, methylene, methine and hydrogen atoms of aromatic rings, respectively 0.86 or 0.82 Å for N-H or O-H bonds. For some of the 26 crystal structures only small weakly diffracting crystals were grown, which caused the B alerts in checkcif evaluation procedure (Li**3b’’**, **5bb** and **8r**). Structures of **5ba** and Li**6’** contain residual electron density (<1 eA^{-3}) in the area of solvent molecules, which result in the B alerts in checkcif evaluation procedure. The solvent molecules in Li**1e** and Li**3b’** were masked by SQUEEZE procedure. In **1c**, the RAHB contact caused a separation of molecules within the dimer, which caused the A alert for not properly connected set of atoms. All mentioned phenomena producing respective alerts have no significant influence to the quality of the structure determination.

Crystallographic data for structural analysis of all compounds have been deposited with the Cambridge Crystallographic Data Centre, CCDC nos. 2417495–2417520. Copies of this information may be obtained free of charge from The Director, CCDC, 12 Union Road, Cambridge CB2 1EY, UK (fax: +44-1223-336033; e-mail: deposit@ccdc.cam.ac.uk or www: http://www.ccdc.cam.ac.uk).

DFT calculations and QTAIM analysis

All the calculations were performed with the Gaussian 16 program.[66] The structures were optimized at the DFT level of theory using the B3LYP[67,68] functional and a standard 6-31g(d,p) basis set with the polarizable continuum model (PCM) used for implicit tetrahydrofuran solvation.[69,70] Transition state (TS) structures of the reaction were found using TS Berny algorithm[71] and QST3[72,73] approach; where the structures of the reactant, product, and estimated TS were used as input for the TS search. The vibrational frequencies and free energies were calculated for all of the optimized structures, and the stationary-point character (a minimum or a first-order saddle point) was thus confirmed. The NMR parameters were calculated using the GIAO method with the 6-311+g(d,p) basis set with PCM. Calculations associated with the dimerization and isomerization mechanism of **1a** were performed at the B3LYP-D3(BJ)/6-311+g(d,p)/PCM(THF) level of theory, dispersion corrections were considered, employing the D3 version of Grimme’s dispersion method.[74]

IR spectroscopy

Infrared (single-bounce diamond ATR) and Raman (vacuum-sealed capillary excitation laser 1064 nm) spectra were recorded on a Nicolet iS50 FTIR spectrometer equipped with the iS50 Raman module.

UV-VIS spectroscopy

Electronic absorption spectra (195−1100 nm) were obtained on Maya2000 Proconcave grating spectrometer using transmission cell with optical path 10 mm with THF and toluene as a solvent at room temperature.

ASSOCIATED CONTENT

Supporting Information. Synthetic procedures, explanation of structures and equilibria, cif files. This material is available free of charge via the Internet at http://pubs.acs.org.

AUTHOR INFORMATION

Corresponding Author

* Eliška Procházková –prochazkova@uochb.cas.cz, Aleš Růžička – ales.ruzicka@upce.cz

Author Contributions

The manuscript was written through contributions of all authors. All authors have given approval to the final version of the manuscript. Stanislava Majerová: synthesis, investigation, writing; Tomáš Chlupatý: NMR spectroscopy, DOSY; Maksim A. Samsonov: DFT; Josef Cvačka: Mass spectrometry; Eliška Procházková: conceptualization, NMR spectroscopy, DFT, writing; Aleš Růžička: conceptualization, supervision, X-ray diffraction analysis, writing.

Funding Sources

This work was supported by the Czech Science Foundation Grant No. 21-02964S. Research infrastructure project CZ.02.01.01/00/23_021/0008593 (Innovative materials suitable for high added value applications (INMA)) is acknowledged.

ACKNOWLEDGMENT

Dr. Martin Novotný and Dr. Petr Švec are acknowledged for some synthetic work and NMR spectroscopic measurements. Assoc. Prof. Dr. Milan Erben for IR spectrum of **PC**.

REFERENCES

1. *Functional Phthalocyanine Molecular Materials*; Jiang, J., Ed.; Structure and Bonding; Springer Berlin Heidelberg: Berlin, Heidelberg, 2010; https://doi.org/10.1007/978-3-642-04752-7.
2. Speck, K.; Magauer, T. The Chemistry of Isoindole Natural Products. *Beilstein J. Org. Chem.* **2013**, *9*, 2048-2078. https://doi.org/10.3762/bjoc.9.243.
3. Radtke, V.; Erk, P.; Sens, B. Isoindoline Pigments. In *High Performance Pigments*; Wiley-VCH, 2009; pp 221-241. https://doi.org/10.1002/9783527626915.ch14
4. Schrage, B. R.; Nemykin, V. N.; Ziegler, C. J. Biliazine Meso Hydrogen Bond: A Ring Open Phthalocyanine Analog With a Meso Hydrogen Bond. *Chem. Commun.* **2020**, *56* (49), 6628-6631. https://doi.org/10.1039/D0CC03060K
5. Costa, R.; Schick, A. J.; Paul, N. B.; Durfee, W. S.; Ziegler, C. J. Hydroxybenziphthalocyanines: Non-Aromatic Phthalocyanine Analogues That Exhibit Strong Uv-Visible Absorptions. *New J. Chem.* **2011**, *35* (4), 794-799. https://doi.org/10.1039/c0nj00500b.
6. Muranaka, A.; Ohira, S.; Hashizume, D.; Koshino, H.; Kyotani, F.; Hirayama, M.; Uchiyama, M. [18]/[20]Π Hemiporphyrazine: A Redox-Switchable Near-Infrared Dye. *J. Am. Chem. Soc.* **2012**, *134* (1), 190-193. https://doi.org/10.1021/ja210410c.
7. Barone, N.; Costa, R.; Sripothangnok, S.; Ziegler, C. J. Dihydroxy- and Tetrahydroxydicarbahemiporphyrazine: Phthalocyanine Analogues With Phenol and Resorcinol Units. *Eur. J. Inorg. Chem.* **2010**, *2010* (5), 775-780. https://doi.org/10.1002/ejic.200900921.
8. Kadam, M. M. L.; Patil, D.; Sekar, N. 4-(Diethylamino) Salicylaldehyde Based Fluorescent Salen Ligand With Red-Shifted Emission – A Facile Synthesis and DFT Investigation. *J. Lumin.* **2018**, No. 204, 354-367. https://doi.org/10.1016/j.jlumin.2018.08.040.
9. Schrage, B. R.; Nemykin, V. N.; Ziegler, C. J. Boshpy Fluorophores: Bodipy Analogues With Single Atom Controlled Aggregation. *Org. Lett.* **2021**, *23* (13), 5246-5250. https://doi.org/10.1021/acs.orglett.1c01776.
10. Dydio, P.; Zieliński, T.; Jurczak, J. Bishydrazide Derivatives of Isoindoline as Simple Anion Receptors. *J. Org. Chem.* **2009**, *74* (4), 1525-1530. https://doi.org/10.1021/jo802288u.
11. Benkó, T.; Lukács, D.; Frey, K.; Németh, M.; Móricz, M. M.; Liu, D.; Kováts, É.; May, N. V.; Vayssieres, L.; Li, M.; Pap, J. S. Redox-Inactive Metal Single-Site Molecular Complexes: A New Generation of Electrocatalysts for Oxygen Evolution? *Catal. Sci. Technol.* **2021**, *11* (19), 6411-6424. https://doi.org/10.1039/D1CY01087E.
12. Grant, E. B.; Guiadeen, D.; Singer, M.; Argentieri, D.; Hlasta, D. J.; Wachter, M. Design, Synthesis, and Biological Activity of Diiminoisoindolines as Complement Component 3A Antagonists. *Bioorg. Med. Chem. Lett.* **2001**, *11* (21), 2817-2820. https://doi.org/10.1016/S0960-894X(01)00522-4.
13. Mombelli, P.; Witschel, M. C.; van Zijl, A. W.; Brun, R.; Diederich, F. Identification of 1,3-Diiminoisoindoline Carbohydrazides as Potential Antimalarial Candidates. *ChemMedChem* **2012**, *7*, 151-158. https://doi.org/10.1002/cmdc.201100441.
14. Clark, P. F.; Elvidge, J. A.; Linstead, R. P. 722. Heterocyclic Imines and Amines. Part II. Derivatives of Isoindoline and Isoindolenine. *J. Chem. Soc. (Resumed)* **1953**, 3593-3601. https://doi.org/10.1039/jr9530003593.
15. Clark, P. F.; Elvidge, J. A.; Golden, J. H. 799. Heterocyclic Imines and Amines. Part Vii. N-Substituted Phthalic Imidine Derivatives and Their Reactions With Amines. *J. Chem. Soc.* **1956**, 4135-4143. https://doi.org/10.1039/jr9560004135.
16. Spiessens, L. I.; Anteunis, M. J. O. NMR Studies on Imidines. V. ^{1}H and ^{13}C Nuclear Magnetic Resonance Study Of The Tautomerism and Geometrical Isomerism of 1,3-Bis(Arylimino)Isoindolines. *Bull. Soc. Chim. Belg.* **1984**, *93* (3), 205-222. https://doi.org/10.1002/bscb.19840930306.
17. Spiessens, L. I.; Anteunis, M. J. O. NMR Studies on Imidines. Vii. The Tautomerism of Mono-N-Aryl Substituted Phthalic Imidines. A ^{1}H and ^{13}C Nuclear Magnetic Resonance Study. *Bull. Soc. Chim. Belg.* **1988**, *97* (6), 431-452. https://doi.org/10.1002/bscb.19880970604.
18. Siegl, W.O. A new bis-cheiating ligand system. Synthesis and chelating behavior. *Inorg. Chim. Acta* **1977**, 25, L65–L66.
19. Tamgho, I. -S.; Engle, J. T.; Ziegler, C. J. The Syntheses and Structures of Bis(Alkylimino)Isoindolines. *Tetrahedron Lett.* **2013**, *54* (45), 6114-6117. https://doi.org/10.1016/j.tetlet.2013.08.134.
20. Camerano, J. A.; Sämann, C.; Wadepohl, H.; Gade, L. H. Bis(Pyridylimino)Isoindolato−Iridium Complexes as Epoxidation Catalysts for Alkenes. *Organometallics* **2011**, *30* (3), 379-382. https://doi.org/10.1021/om1010116.
21. Müller, A. L.; Bleith, T.; Roth, T.; Wadepohl, H.; Gade, L. H. Iridium Half-Sandwich Complexes With Di- And Tridentate Bis(Pyridylimino)Isoindolato Ligands: Stoichiometric and Catalytic Reactivity. *Organometallics* **2015**, *34* (11), 2326-2342. https://doi.org/10.1021/om501138t.
22. Müller, A. L.; Wadepohl, H.; Gade, L. H. Bis(Pyridylimino)Isoindolato (Bpi) Osmium Complexes: Structural Chemistry and Reactivity. *Organometallics* **2015**, *34* (12), 2810-2818. https://doi.org/10.1021/acs.organomet.5b00080.
23. Sauer, D. C.; Kruck, M.; Wadepohl, H.; Enders, M.; Gade, L. H. Spin Density Distribution In Iron(Ii) and Cobalt(Ii) Alkyl Complexes Containing 1,3-Bis(2-Pyridylimino)Isoindolate Ligands. *Organometallics* **2013**, *32* (3), 885-892. https://doi.org/10.1021/om301198b.
24. Schrage, B. R.; Vitale, D.; Kelly, K. A.; Nemykin, V. N.; Herrick, R. S.; Ziegler, C. J. Binding A Meridional Ligand in a Facial Geometry: A Square Peg in a Round Hole. *J. Organomet. Chem.* **2020**, *919*, 121331. https://doi.org/10.1016/j.jorganchem.2020.121331.
25. Martić, G.; Engle, J. T.; Ziegler, C. J. Complexes of 1,3-Bis(2-Thiazolylimino)Isoindoline With Middle and Late First Row Transition Metals. *Inorg. Chem. Commun.* **2011**, *14* (11), 1749-1752. https://doi.org/10.1016/j.inoche.2011.08.001.
26. Osinski, A. J.; Morris, D. L.; Herrick, R. S.; Ziegler, C. J. Re(Co) 3 -Templated Synthesis Of A-Amidinoazadi(Benzopyrro)Methenes. *Inorg. Chem.* **2017**, *56* (24), 14734-14737. https://doi.org/10.1021/acs.inorgchem.7b02140.
27. Sevov, C. S.; Fisher, S. L.; Thompson, L. T.; Sanford, M. S. Mechanism-Based Development of a Low-Potential, Soluble, and Cyclable Multielectron Anolyte for Nonaqueous Redox Flow Batteries. *J. Am. Chem. Soc.* **2016**, *138*, 15378-15384. https://doi.org/10.1021/jacs.6b07638.
28. Maleev, A. A.; Balashova, T. V.; Fukin, G. K.; Katkova, M. A.; Lopatin, M. A.; Bochkarev, M. N. 1,3-Bis(Alkylimino)Isoindolinates of Rare Earth Metals: Synthesis, Molecular Structure and Photoluminescence. *Polyhedron* **2010**, *29* (1), 10-15. https://doi.org/10.1016/j.poly.2009.05.020.
29. Edelmann, F. T. Recent Progress in the Chemistry of Metal Amidinates and Guanidinates. In Advances in Organometallic Chemistry; Adv. Organomet. Chem.; Elsevier, 2013; pp 55-374. https://doi.org/10.1016/B978-0-12-407692-1.00002-3.
30. Collins, S. Polymerization Catalysis With Transition Metal Amidinate And Related Complexes. *Coord. Chem. Rev.* **2011**, *255* (1-2), 118-138. https://doi.org/10.1016/j.ccr.2010.07.005.
31. Edelmann, F. T. Lanthanide Amidinates and Guanidinates In Catalysis and Materials Science: A Continuing Success Story. *Chem. Soc. Rev.* **2012**, *41* (23), 7657-7672. https://doi.org/10.1039/c2cs35180c.
32. Novotný, M.; Švec, P.; Růžičková, Z.; Růžička, A. Structure of Non-Symmetric Lithium Amidinate Complexes Prepared by Addition of Lithium Amides to Various Nitriles. *J. Organomet. Chem.* **2017**, *828*, 68-74. https://doi.org/10.1016/j.jorganchem.2016.11.015.

33. Novotný, M.; Švec, P.; Růžičková, Z.; Růžička, A. Direct Access to Non-Symmetric Lithium Nitriloamidinate and Disymmetric Dilithium Bisamidinate Complexes From 1,3- Or 1,4- Dicyanobenzene and Lithium Amides. *J. Organomet. Chem.* **2017**, *849-850*, 88-97. https://doi.org/10.1016/j.jorganchem.2017.09.008.
34. Cissell, J. A.; Vaid, T. P.; Yap, G. P. A. The Doubly Oxidized, Antiaromatic Tetraphenylporphyrin Complex [Li(Tpp)][Bf 4]. *Org. Lett.* **2006**, *8* (11), 2401-2404. https://doi.org/10.1021/ol060772l.
35. Pyykkö, P.; Atsumi, M. Molecular Double-Bond Covalent Radii for Elements Li–E112. *Chem. – Eur. J.* **2009**, *15* (46), 12770-12779. https://doi.org/10.1002/chem.200901472.
36. Shishkin, O. V.; Konovalova, I. S.; Hordiyenko, O. V.; Leszczynski, J. Remarkably Strong Polarization of Amidine Fragment in the Crystals of 1-Imino-1H-Isoindol-3-Amine. *Struct. Chem.* **2013**, *24* (4), 1089-1097. https://doi.org/10.1007/s11224-012-0131-y.
37. Zhang, Z. -Q.; Njus, J. M.; Sandman, D. J.; Guo, C.; Foxman, B. M.; Erk, P.; van Gelder, R. Diiminoisoindoline: Tautomerism, Conformations, and Polymorphism. *Chem. Comm.* **2004**, No. 7, 886-887. https://doi.org/10.1039/b400111g.
38. Bore, J.; Chen, W. -Y.; Nemykin, V. N.; Ziegler, C. J. Imino(Dialkylamino)Isoindolines: Structures and Dynamic Behavior. *J. Porphyr. Phthaloc.* **2024**, *28* (07), 429-434. https://doi.org/10.1142/S1088424624500317.
39. Zhang, Z. -Q.; Uth, S.; Sandman, D. J.; Foxman, B. M. Structure, Polymorphism and Thermal Properties of Phenyliminoisoindolines. *J. Phys. Org. Chem.* **2004**, *17* (9), 769-776. https://doi.org/10.1002/poc.793.
40. Gilli, G.; Bellucci, F.; Ferretti, V.; Bertolasi, V. Evidence for Resonance-Assisted Hydrogen Bonding from Crystal-Structure Correlations on the Enol Form of the .Beta.-Diketone Fragment. *J. Am. Chem. Soc.* **1989**, *111* (3), 1023-1028. https://doi.org/10.1021/ja00185a035.
41. Bertolasi, V.; Gilli, P.; Ferretti, V.; Gilli, G. Evidence for Resonance-Assisted Hydrogen Bonding. 2. Intercorrelation Between Crystal Structure and Spectroscopic Parameters in Eight Intramolecularly Hydrogen Bonded 1,3-Diaryl-1,3-Propanedione Enols. *J. Am. Chem. Soc.* **1991**, *113* (13), 4917-4925. https://doi.org/10.1021/ja00013a030.
42. Gilli, P.; Bertolasi, V.; Ferretti, V.; Gilli, G. Evidence for Resonance-Assisted Hydrogen Bonding. 4. Covalent Nature of the Strong Homonuclear Hydrogen Bond. Study of the O-H--O System by Crystal Structure Correlation Methods. *J. Am. Chem. Soc.* **1994**, *116* (3), 909-915. https://doi.org/10.1021/ja00082a011.
43. Homborg, H.; Teske, C. L. Lithiumphthalocyanine: Darstellung und Charakterisierung der Monoklinen und Tetragonalen Modifikationen Von Lipc(1-) und der Halogenaddukte Lipc(1-)X (X = Cl, Br, I). *Z. anorg. allg. Chem.* **1985**, *527* (8), 45-61. https://doi.org/10.1002/zaac.19855270805.
44. Zanotti, G.; Palmeri, F.; Raglione, V. Phthalocyanines Synthesis: A State-of-the-Art Review of Sustainable Approaches Through Green Chemistry Metrics. Chem. Eur. J. **2024**, 30 (44). https://doi.org/10.1002/chem.202400908.
45. Pap, J. S.; Kripli, B.; Bányai, V.; Giorgi, M.; Korecz, L.; Gajda, T.; Árus, D.; Kaizer, J.; Speier, G. Tetra-, Penta- and Hexacoordinate Copper(II) Complexes With N3 Donor Isoindoline-Based Ligands: Characterization and Sod-Like Activity. *Inorganica Chim. Acta* **2011**, *376* (1), 158-169. https://doi.org/10.1016/j.ica.2011.06.001.
46. Kripli, B.; Baráth, G.; Balogh-Hergovich, É.; Giorgi, M.; Simaan, A. J.; Párkányi, L.; Pap, J. S.; Kaizer, J.; Speier, G. Correlation Between The Sod-Like Activity of Hexacoordinate Iron(Ii) Complexes and Their Fe3+/Fe2+ Redox Potentials. *Inorg. Chem. Commun.* **2011**, *14* (1), 205-209. https://doi.org/10.1016/j.inoche.2010.10.023.
47. Pap, J. S.; Bányai, V.; Szilvási, D. S.; Kaizer, J.; Speier, G.; Giorgi, M. Influence of Meridional N3-Ligands on Supramolecular Assembling and Redox Behavior of Carboxylatocopper(II) Complexes. *Inorg. Chem. Commu.* **2011**, *14* (11), 1767-1772. https://doi.org/10.1016/j.inoche.2011.08.005.
48. Kaizer, J.; Kripli, B.; Speier, G.; Párkányi, L. Synthesis, Structure, and Catalase-Like Activity of a Novel Manganese(II) Complex: Dichloro[1,3-Bis(2′-Benzimidazolylimino)Isoindoline]Manganese(Ii). *Polyhedron* **2009**, *28* (5), 933-936. https://doi.org/10.1016/j.poly.2009.01.008.
49. Bröring, M.; Kleeberg, C.; Cónsul Tejero, E. Syntheses, Structures and Coordination Modes of Acetatopalladium(II) Complexes With 1,3-Bis(2-Arylimino)Isoindoline Ligands of Different Steric Influence. *Eur. J. Inorg. Chem.* **2007**, *2007* (20), 3208-3216. https://doi.org/10.1002/ejic.200700286.
50. Bretschneider, A.; Andrada, D. M.; Dechert, S.; Meyer, S.; Mata, R. A.; Meyer, F. Preorganized Anion Traps for Exploiting Anion–Π Interactions: An Experimental and Computational Study. *Chem. Eur. J.* **2013**, *19* (50), 16988-17000. https://doi.org/10.1002/chem.201302598.
51. Kurzer, F.; Douraghi-Zadeh, K. Advances in the Chemistry of Carbodiimides. *Chem. Rev.* **1967**, *67*(2), 107-152. https://doi.org/10.1021/cr60246a001.
52. Alonso-Moreno, C.; Antiñolo, A.; Carrillo-Hermosilla, F.; Otero, A. Guanidines: From Classical Approaches yo Efficient Catalytic Syntheses. *Chem. Soc. Rev* **2014**, *43*(10), 3406-3425. https://doi.org/10.1039/C4CS00013G.
53. Koller, J.; Bergman, R. G. Highly Efficient Aluminum-Catalyzed Hydro-Amination/-Hydrazination of Carbodiimides. *Organometallics* **2010**, *29* (22), 5946-5952. https://doi.org/10.1021/om100735q.
54. Zhou, S.; Wang, S.; Yang, G.; Li, Q.; Zhang, L.; Yao, Z.; Zhou, Z.; Song, H. -bin. Synthesis, Structure, and Diverse Catalytic Activities of [Ethylenebis(Indenyl)]Lanthanide(III) Amides On N−H and C−H Addition to Carbodiimides and E -Caprolactone Polymerization. *Organometallics* **2007**, *26* (15), 3755-3761. https://doi.org/10.1021/om070234s.
55. Shen, H.; Chan, H. -S.; Xie, Z. Guanylation of Amines Catalyzed by a Half-Sandwich Titanacarborane Amide Complex. *Organometallics* **2006**, *25* (23), 5515-5517. https://doi.org/10.1021/om060811x.
56. Montilla, F.; del Río, D.; Pastor, A.; Galindo, A. Use of Vanadium Complexes as Catalysts in the Synthesis of Guanidines: New Experimental Data and DFT Analysis of the Carbodiimide Interaction With the Catalyst. *Organometallics* **2006**, *25* (21), 4996-5002. https://doi.org/10.1021/om060535m.
57. Gilli, P.; Bertolasi, V.; Pretto, L.; Lyčka, A.; Gilli, G. The Nature of Solid-State N−H···o/O−H···n Tautomeric Competition in Resonant Systems. Intramolecular Proton Transfer in Low-Barrier Hydrogen Bonds Formed by the ···Oc−Cn−Nh··· ⇄ ···Ho−Cc−Nn··· Ketohydrazone−Azoenol System. A Variable-Temperature X-Ray Crystallographic and DFT Computational Study. *J. Am. Chem. Soc.* **2002**, *124* (45), 13554-13567. https://doi.org/10.1021/ja020589x.
58. Pantoş, G. D.; Rodríguez-Morgade, M. S.; Torres, T.; Lynch, V. M.; Sessler, J. L. 2-Amino-3,4-Diethylpyrrole Derivatives: New Building Blocks for Coiled Structures. *Chem. Commun* **2006**, No. 20, 2132-2134. https://doi.org/10.1039/B602956F.
59. Huber, S. M.; Mata, G.; Linden, A.; Luedtke, N. W. Synthesis and Structure of a Hydrogenated Zinc Hemiporphyrazine. *Chem. Commun* **2013**, *49* (39), 4280-4282. https://doi.org/10.1039/C2CC37151K.
60. Çetin, A.; Durfee, W. S.; Ziegler, C. J. Low-Coordinate Transition-Metal Complexes of a Carbon-Substituted Hemiporphyrazine. *Inorg. Chem.* **2007**, *46* (16), 6239-6241. https://doi.org/10.1021/ic7011099.
61. Costa, R.; Engle, J. T.; Ziegler, C. J. The Synthesis and Metal Binding Chemistry of Carbahemiporphyrazines With an Electron Withdrawing Substituent. *J. Porphyr. Phthalocya.* **2012**, *16* (2), 175-182. https://doi.org/10.1142/S1088424612004835.
62. Krause, L.; Herbst-Irmer, R.; Sheldrick, G. M.; Stalke, D., Comparison of silver and molybdenum microfocus X-ray sources for

single-crystal structure determination. *J. Appl. Crystallogr.* **2015,** *48* (1), 3-10. https://doi.org/10.1107/S1600576714022985

63. Sheldrick, G., SHELXT - Integrated space-group and crystal-structure determination. *Acta Cryst.* **2015,** *A71* (1), 3-8. https://doi.org/10.1107/S2053273314026370
64. Sheldrick, G., Crystal structure refinement with SHELXL. *Acta Cryst.* **2015,** *C71* (1), 3-8. https://doi.org/10.1107/S2053229614024218
65. Bruker-AXS *APEX4 v2022.1-1*, 2022.
66. Frisch, M. J.; Trucks, G. W.; Schlegel, H. B.; Scuseria, G. E.; Robb, M. A.; Cheeseman, J. R.; Scalmani, G.; Barone, V.; Petersson, G. A.; Nakatsuji, H.; Li, X.; Caricato, M.; Marenich, A. V.; Bloino, J.; Janesko, B. G.; Gomperts, R.; Mennucci, B.; Hratchian, H. P.; Ortiz, J. V.; Izmaylov, A. F.; Sonnenberg, J. L.; Williams; Ding, F.; Lipparini, F.; Egidi, F.; Goings, J.; Peng, B.; Petrone, A.; Henderson, T.; Ranasinghe, D.; Zakrzewski, V. G.; Gao, J.; Rega, N.; Zheng, G.; Liang, W.; Hada, M.; Ehara, M.; Toyota, K.; Fukuda, R.; Hasegawa, J.; Ishida, M.; Nakajima, T.; Honda, Y.; Kitao, O.; Nakai, H.; Vreven, T.; Throssell, K.; Montgomery Jr., J. A.; Peralta, J. E.; Ogliaro, F.; Bearpark, M. J.; Heyd, J. J.; Brothers, E. N.; Kudin, K. N.; Staroverov, V. N.; Keith, T. A.; Kobayashi, R.; Normand, J.; Raghavachari, K.; Rendell, A. P.; Burant, J. C.; Iyengar, S. S.; Tomasi, J.; Cossi, M.; Millam, J. M.; Klene, M.; Adamo, C.; Cammi, R.; Ochterski, J. W.; Martin, R. L.; Morokuma, K.; Farkas, O.; Foresman, J. B.; Fox, D. J. *Gaussian 16 Rev. C.01*, Wallingford, CT, 2016.
67. Becke, A. D. Density-Functional Thermochemistry. Iii. The Role Of Exact Exchange. *J. Chem. Phys.* **1993**, *98* (7), 5648-5652. https://doi.org/10.1063/1.464913.
68. Lee, C.; Yang, W.; Parr, R. G. Development of The Colle-Salvetti Correlation-Energy Formula Into A Functional Of The Electron Density. *Phys. Rev.* **1988**, *B37* (1), 785-789. https://doi.org/10.1103/PhysRevB.37.785.
69. Barone, V.; Cossi, M. Quantum Calculation of Molecular Energies And Energy Gradients In Solution By A Conductor Solvent Model. *J. Phys. Chem.* **1998**, *A102* (11), 1995-2001. https://doi.org/10.1021/jp9716997.
70. Schlegel, H. B. Optimization Of Equilibrium Geometries And Transition Structures. *J. Comput. Chem.* **1982**, *3* (2), 214-218. https://doi.org/10.1002/jcc.540030212.
71. Cossi, M.; Rega, N.; Scalmani, G.; Barone, V. Energies, Structures, And Electronic Properties of Molecules In Solution With The C-Pcm Solvation Model. *J. Comput. Chem.* **2003**, *24* (6), 669-681. https://doi.org/10.1002/jcc.10189.
72. Peng, C.; Ayala, P.; Shlegel, H.; Frisch, M. Using Redundant Internal Coordinates To Optimize Equilibrium Geometries And Transition States. *J. Comput. Chem* **1996**, *17* (1), 49-56. https://doi.org/10.1002/(SICI)1096-987X(19960115)17:1<49::AID-JCC5>3.0.CO;2-0
73. Peng, C.; Bernhard Schlegel, H. Combining Synchronous Transit and Quasi-Newton Methods To Find Transition States. *Isr. J. Chem.* **1993**, *33* (4), 449-454. https://doi.org/10.1002/ijch.199300051.
74. Grimme, S.; Antony, J.; Ehrlich, S.; Krieg, H. A Consistent And Accurate Ab Initio Parametrization Of Density Functional Dispersion Correction (Dft-D) For The 94 Elements H-Pu. *J. Chem. Phys.* **2010**, *132* (15), 154104. https://doi.org/10.1063/1.3382344.

For table of contents only

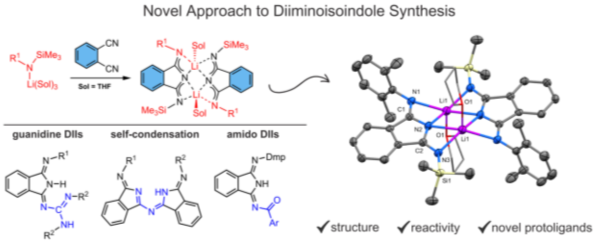

Synopsis text

Various diiminoisoindoles and its derivatives were prepared by reaction of 1,2-dicyanobenzene and silylated lithium amides. Follow-up reactivity such as protonolysis, condensation, addition or C-N coupling was studied. *E*/*Z*-isomerism, tautomerism and agglomeration of compounds were described in solution and solid state. Possibilities to use such compounds as ligands in coordination chemistry are documented by presence of resonance-assisted hydrogen bonds and formation of lithium complexes.